RSC Advances

PAPER

View Article Online
View Journal | View Issue

Cite this: *RSC Adv.*, 2022, **12**, 9179

Fabrication and characterization of a toughened spherical chitosan adsorbent only through physical crosslinking based on mechanism of Chain Rearrangement

Cai-Hong Liu, Hai-Tao Jiang and Chun-Hong Wang*

Chitosan extracted from natural products has gained tremendous attention in the field of adsorption and separation due to its inherent biocompatibility and potential applications. In this research, we synthesized a new type of spherical chitosan adsorbent (SCA) by controlling the mass transfer rate of the entanglement of the polymer chains in the recombination process. This SCA is a highly crystalline polymer material with outstanding mechanical strength, high adsorption capacity, a porous surface and suitable particle size distribution. The value of the sphericity of attrition of this SCA was 89.8%, which is the same as that of the commercial macroporous resin with a polystyrene matrix. The X-ray diffraction (XRD) patterns and differential scanning calorimetry (DSC) curves showed a significant change from powder to spherical structure and confirmed that the SCA is highly ordered and crystalline. Optical microscopy (OM) and scanning electron microscopy (SEM) demonstrated that the SCA was composed of a tightly stacked fiber structure, indicating the homogeneity of the polymerization. The porous structure of the surface provided a channel for mass transfer, which was indicated by a test of the ion exchange capacity and the adsorption performance of the SCA with Cu(II) as the adsorbed subject. The adsorption capacity was higher than those of all reported non-composite chitosan materials. Therefore, we have successfully synthesized a completely green, nontoxic and environmentally friendly adsorbing resin equipped with excellent mechanical properties and adsorption capacity for future applications in many new fields.

Received 30th December 2021
Accepted 22nd February 2022

DOI: 10.1039/d1ra09438f

rsc.li/rsc-advances

Introduction

Ion exchange resin is a widely used functional polymer material. The basic skeleton of the resin undergoes a transformation from phenolic to polystyrene and acrylate. Most polymerized monomers are derived from petroleum.[1,2] The polymerization process of nondegradable and nonrenewable polymers causes pollution and energy consumption. Recently, the concept of fossil fuel-free, environmentally friendly materials and recycled and reused materials has been listed as one of the 125 international frontiers, and research on biocompatible and biodegradable natural polymer replacements has attracted much attention.[3]

Chitosan is the only basic polysaccharide that exists in nature and is widely used due to its abundant hydroxyl and amino groups on the main chain.[4] Therefore, the large-scale industrial production of this environmentally friendly adsorption material can lower manufacturing costs and reduce the waste of resources to a great extent. However, chitosan powder is difficult to reuse and separate in practical applications,[5] so it needs to be reprocessed. Spherical adsorbent fillers have the advantages of high volumetric capacity and uniform stress and strain, and they can achieve a higher filling volume by adjusting the diameter and size distribution.[6] Therefore, some scholars have committed themselves to the synthesis and research of spherical chitosan resin.[7–11] Most of these scholars have established a three-dimensional network structure by introducing chemical cross-linking agents and with amino groups as reactive cross-linking sites, resulting in a decrease in available functional groups in the processed materials.[12] To increase the adsorption performance, current research has mainly focused on the modification of the synthesis of the material by physical cross-linking.[13–16] In the reported methods, the high concentration of hydroxide ions gathered on the surface causes physical gelation to occur preferentially at the outermost shell, the diffusion of ions to the inner layer is hindered, and the result is a low rate of transformation, which contributes to the softness of the interior. The material with this structure cannot withstand external impact and abrasion when used as resin packed in columns.

Key Laboratory of Functional Polymer Materials (Ministry of Education), College of Chemistry, Nankai University, Tianjin 300071, P. R. China. E-mail: wch2004@nankai.edu.cn

For decades, to increase the conversion degree, some research papers have reported the preparation of novel chitosan biohydrogels by purely physical cross-linking.[17,18] Zhang[19] dissolved chitosan in alkali/urea solutions at low temperature rather than in acidic systems to obtain high-strength hydrogels with nanofibrous structures. Ladet[20] synthesized a multilayer chitosan gel material with a directional structure through the difference in the concentration gradient of hydroxide at the gel–sol interface in a cylindrical mold. By controlling the gelation and the OH^- diffusion time, the polymer chains of the two types of materials mentioned above can be rearranged more regularly, thereby improving the overall mechanical strength.

From the perspective of adsorption and separation material, we hope the processed chitosan met the following conditions, a complete sphere with the relatively homogeneous and controllable particle size, the strength equivalent to that of polystyrene ion exchange resin and good mass transfer channels existing inside, and as much functional group content retained as possible. Its crystallization can be controlled by providing suitable external conditions during processing.[21] The crystallization rate affects the degree of crystallinity and the distribution of regions, which affects both the mechanical properties and usability of functional groups.[22,23] Fast crystallization contributes to the uniform distribution of the crystalline area, but the strength of the resin declined for the reduction in crystallinity.; slowing down the rate in favour of increasing the degree of crystallisation, but the presence of a large proportion of crystalline zones correspondingly reduces the content of the functional group. Here, we provide suitable crystallization conditions at higher reactant concentrations to generate spherical crystalline polymers that aggregate steadily in one phase. The crystallization rate was decreased by slowing down the variation rate of the pH so that the polymer chains could fully reorganize inside the beads; this organization enabled the crystalline area to be distributed among the interchain spaces of the adsorbent rather than only on the surface. In addition, the presence of water as a pore-foaming agent can create the channel for mass transfer to ensure sufficient functional groups are available.

In this study, we synthesized a spherical chitosan adsorbent (SCA) by water-in-oil reversed-phase suspension polymerization. The chitosan powder was dissolved in an aqueous acetic acid solution as the dispersed phase, while the continuous phase was a combination of butyl acetate and dichloroethane, which were chosen based on density and polarity. The proportion of the compounds can ensure that the density of the two phases is consistent and the polarity can ensure that the monomer microdroplets can be suspended in the oil phase and emulsification does not occur in the polymerization process. In the alkalization of the solid phase precipitation of small droplets, we control the rate of alkali ions entering the system by adding sodium chloride. Due to the common ion effect and salting-out effect,[24,25] sodium chloride can simultaneously reduce the solubility of the alkali and the polymer in the solvent, which is equivalent to establishing a barrier among the molecular chain. By delaying the reorganization of molecular chains, for the first time, we synthesized a highly crystalline spherical chitosan resin with a polycrystalline region distribution supporting the three-dimensional architecture and its porous surface, providing a channel for mass transfer. The particle size can be controlled in the range of 100–1000 μm, and the sphericity after attrition is 89.8%, which is equal to that of the commercial adsorption resin and has met industrial requirements. It can be used as a weakly basic anion exchange resin with an amino exchange capacity from 5.9 to 6.2 mmol g^{-1} and a chelating resin by absorbing Cu(II) to 200.0 mg g^{-1} for 24 h, and it has numerous potential applications in many fields.

Experimental section

Materials

Raw chitosan powder (degree of deacetylation ≥95%) was purchased from MERYER Co., Ltd (Shanghai, China), and the viscosity-averaged molecular weight (M_μ) was 200–800 MPa s^{-1}. Butyl acetate and acetic acid (99.7+%, ACS reagent grade) were obtained from Aladdin Co., Ltd (Shanghai, China) and used as received. HCl, NaCl, NaOH, ethanol, Span 80, dichloromethane and copper sulfate pentahydrate (Tianjin Bohua Chemical Reagents Co., Ltd, China) were of analytical grade and used without further purification.

Synthesis of the SCA

The chitosan solution was prepared by dissolving the purified chitosan powder in HAC/H_2O (1 : 23 by weight). A transparent chitosan (TC) solution with a concentration of 4 wt% was obtained. Subsequently, a well-mixed suspension containing 240 mL dichloroethane and 250 mL butyl acetate was dispersed in a three-necked round-bottom flask. Then, 4.9 mL Span 80 was added as a dispersant and stirred for 10 min at 25 °C. Later, 130 mL of the viscous TC solution was poured into the suspension, which was stirred at 230 rpm for 4 h in a water bath at 25 °C to generate small, stable water/oil droplets. After droplets with a round shape and suitable diameter were obtained, 1–2 mL prepared saturated sodium chloride solution was dropped into the flask and diffused throughout the entire system. Afterward, an alkali curing agent of NaOH/NaCl/H2O (22 : 7:20 by weight) was added 1 mL every half hour into the suspension. The degree of neutralization gradually increased the refractive index of the droplets. After 4 hours, the solidified spherical polymers all sank to the bottom of the flask, successfully illustrating the transition in the aggregated structure of the chitosan from powder to spherical resin. Furthermore, the chitosan absorbent was rinsed with deionized water until the pH was neutral.

Characterization of the SCA

To prove that polymer chain reaggregation did not only occur on the surface, the morphologies of chitosan from the droplets to beads were observed with an optical microscope. They were photographed every half hour to record and observe changes in their physical properties. The morphologies and structures of the surfaces and cross sections of the SCA were observed with cold field emission scanning electron microscopy (JSM-7500F,

AEMC) and wide-angle X-ray diffraction (XRD, Rigaku, SmartLab). The acceleration voltage for the SEM observation was 5 kV. The SCA was lyophilized in a freeze-dryer for SEM observation. The surface and cross section of the beads were sputtered with gold and then observed. XRD patterns with Cu Kα radiation at 40 kV and 150 mA were recorded in the 2θ region from 5° to 40°. The samples included freeze-dried SCA beads and chitosan powder dried in a vacuum oven at 60 °C for 48 h. The peak position and crystallinity index of the samples were obtained by peak fitting. Solid-state phase transformations in the aggregation were studied using differential scanning calorimetry (DSC). DSC measurements were performed (−40 to 300 °C) on a DSC-204 calorimeter (STA 449 F3, NETZSCH Group) at a heating rate of 10 °C min^{-1} under a nitrogen atmosphere, flowing at 100 mL min^{-1}. The strength of the SCA was measured from the sphericity after attrition.

Determination for the sphericity after attrition

Referring to GB/T 12598-2001, the strength analysis of ion exchange resin was determined by measuring the sphericity after attrition. Measure 50 mL of resin sample in 100 mL measuring cylinder, retain 5 mL of pure water on top of the resin. Transfer all resin in the measuring cylinder to the drum with 145 mL of pure water and add 10 porcelain balls. Mill for 30 min, then transfer all resin with pure water and dry at 60 °C. Place the dry sample to the enamel pan, tilt the enamel pan at an angle that allows the round ball particles to roll off in gentle vibration without the broken particles rolling off. Gently poke a small portion of the resin with a brush to separate the round ball particles from the broken particles, brushing the broken particles. In the separated specimen, the remaining broken particles in the round sphere particle part should be less than 50, and the remaining round sphere particles in the broken particle part should also be less than 50. Weigh the round spherical particles and broken particles on the analytical balance, record the mass of round spherical particles and broken particles as m_1 and m_2. The sphericity after attrition (A) of the chitosan samples was determined using the equation.

$$A = \frac{m_1}{m_1 + m_2} \times 100 \quad (1)$$

where m_1 and m_2 stand for the mass of intact and broken beads, g.

Ion exchange capacity

When the SCA reacts with an excessively strong monobasic acid (hydrochloric acid), the content of available amino groups in the SCA can be calculated based on the amount of unreacted acid. According to the "Determination for exchange capacity of anion exchange resins in hydroxylic form" of GB/T 5760-2000, before the neutralization treatment, 1.0 g of centrifuged solution was mixed with 50 mL 0.1 M HCl–NaCl standard solution in a clean and stoppered Erlenmeyer flask to remove external moisture beads. Next, the mixed solution was warmed in a constant temperature water bath oscillator at 40 °C for 2 h and then cooled to room temperature. A dilute aqueous NaOH solution with a nominal concentration of 0.1 M was freshly prepared just before use, and acidity of the supernatant was determined by an acid–base titration with phenolphthalein as the indicator. The amino exchange capacity of the SCA was calculated by the following formula.

$$Q = \frac{50 \times N_1 - N_2 \times V}{W \times (1 - X)} \quad (2)$$

where Q is the exchange capacity of the SCA, mmol g^{-1}; N_1 is the concentration of the standard hydrochloric acid and sodium chloride titration solutions, mmol L^{-1}; N_2 is the accurate concentration of the dilute NaOH solution with a nominal concentration of 0.1 M, mmol L^{-1}; W is the mass of SCA, typically 1.0 g; V is the volume of sodium hydroxide standard titration solution neutralized by the titration supernatant, L; X is the moisture content of the SCA measured with a moisture analyzer (Sartorius, Germany), %.

Adsorption performance of the SCA

Herein, copper, frequently selected as the metal to coordinate with amine chelating resin, was used as a model to investigate the adsorption characteristics of the SCA. Batch adsorption experiments were carried out in a shaker outfitted with a thermostat by shaking 1.0 g of centrifuged solution to remove external moisture from the resin with 50 mL of an aqueous solution of cupric ions at the desired concentration, pH, and temperature in a 120 mL flask. Inductively coupled plasma-optical emission spectroscopy (ICP-OES, Agilent 5110) was used to detect the Cu(II) in the supernatant before and after adsorption. In the adsorption experiment,[26] the amount of Cu(II) adsorbed onto the SCA (Q, mg g^{-1}) was determined using the equation.

$$Q = \frac{V \times (c_o - c_n)}{W \times (1 - X)} \quad (3)$$

where V is the volume of adsorption solution, L; c_0 is the initial concentration of metal ions; c_x is the value after x hours of adsorption, mg L^{-1}; W is the weight of the SCA, g; and X is the moisture content of the SCA, %.

Results and discussion

Optical microscopy (OM) analysis

We provide evidence to prove that the synthesis of spherical chitosan resin materials is a gradual and homogeneous process. The OM photomicrographs in Fig. 1 visually show the morphological changes during the process of preparing the SCA. The addition of NaCl prevented the diffusion of NaOH from the oil phase to the polymer, resulting in a decreasing polyreaction rate of the whole phase. In the beginning, the droplets (Fig. 1a) dispersed by shear force were irregular when they were observed by OM to be leaving the polymerization system. As neutralization proceeded, the polymer chain segment rearrangement and interactions favoured the formation of a stable conformation of polymers.[27] The curvature became more uniform, and the shape of the material became

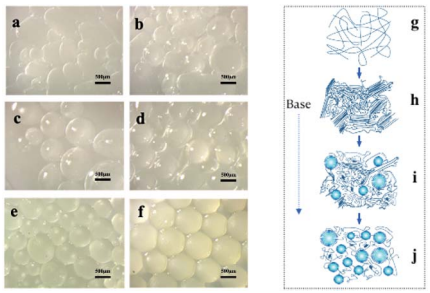

Fig. 1 OM photomicrographs of the SCA in the intermediate state of different periods in sequence (a–e) and final state (f). (g) to (j) show the process of the Chain Rearrangement.

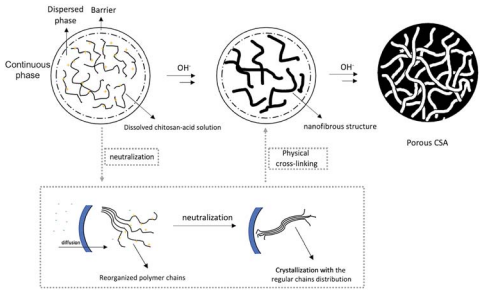

Fig. 3 Overview of the rearrangement of polymer chains in the presence of a barrier.

spherical (Fig. 1b–e). Fig. 1e shows the state in which the morphology was fixed and did not collapse after phase separation. In a comparison of Fig. 1e and f, it can be seen that the refractive index of the resin of Fig. 1f greatly increased, and that this material had a higher crystallinity. As shown in Fig. 2, we can obtain the size of the SCA vary from 250 to 830 μm in diameter.

Formation mechanism

The molecular chains of the dissolved chitosan are disorderly dispersed in acidic aqueous solution (Fig. 1g). In the presence of a saturated salt solution, as mentioned earlier, acid-base neutralization reacts slowly to ensure that there is enough time for chains to aggregate regularly while forming crystal nuclei (Fig. 1h). As nucleation and crystal growth proceed in a concentrated polymer solution, polycrystalline aggregates—spherulites—eventually form.[22] Of course, new crystal nuclei are generated simultaneously (Fig. 1i). The reaction is complete when the crystal nuclei have all grown into spherulites (Fig. 1j). The result shows that the distance between adjacent spherulites becomes shorter and the cross-linked network becomes much denser, which demonstrates that a material with outstanding crystallinity and mechanical properties forms. The porous surface of the final structure is formed, with water as a pore-foaming agent (Fig. 3).[28]

Fiber network formation process

The internal structure of the materials was observed by using a scanning electron microscope (SEM). We removed the droplets at different times of the reaction and then chose the cut section for observation. The SEM image of Fig. 4a revealed the initial crumbly internal texture. A higher aggregation degree can be seen in Fig. 4b, and regular arrangement among molecular chains started to appear in Fig. 4c. More specifically, crystal nuclei began to be generated as a cross-linking medium. Later, the two processes simultaneously formed crystals and made the polymer present a locally regular intermediate structure (Fig. 4d). Fig. 4e shows that the aggregates had a well-ordered lamellar structure, while Fig. 4f shows that at the same magnification, the sample was already in the form of a polymer with a complete structure.[29] The images in Fig. 4g–j were observed at higher magnifying power. The self-assembly process of stacking polymer chains was more intuitive. We vividly described the structure in Fig. 4g as a paste-like collapsed morphology. Fig. 4h–j show the appearance of a local three-dimensional structure, as well as the formation and close packing of the phase-integrated fiber network. Fig. 4k shows that the XRD patterns of the SCA differed throughout the homogeneous reaction. Several crystal reflections could be observed in the range of 5–40°. They were indexed as 020, 110 and 130, and the overall peak intensity increased gradually in proportion to the extent of reaction.[30] The maximum peak of intensity of the 110° reflection increased from no. 3 and moved to a higher angle to no. 12, and the second maximum peak of intensity at 020° reflection also increased obviously from no. 10–12. Therefore, the XRD results successfully showed that the crystallinity degree improved during the formation of the SCA.[11]

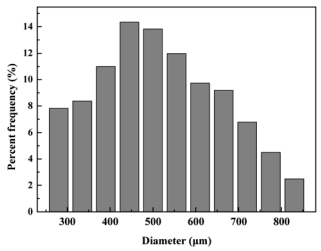

Fig. 2 The size distribution of the SCA.

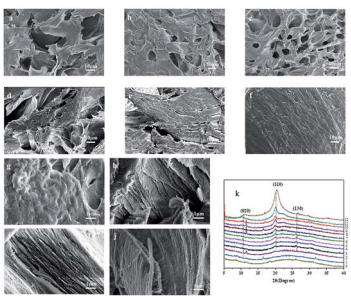

Fig. 4 SEM images of the inner configuration of the SCA with different degrees of reaction (a–j). (k) Comparison of X-ray diffractograms of the SCA at different stages of synthesis. The samples from bottom to top are samples 0–12, respectively.

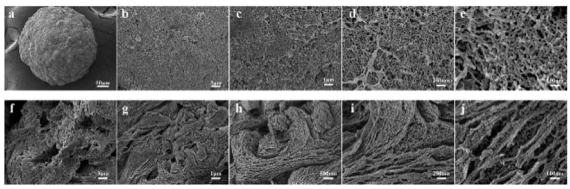

Fig. 5 SEM images of the representative surface (a–e) and cross-sectional structure (f–j) of the SCA.

In Fig. 5a, the SCA exhibited a spherical shape with a mean diameter of 500 μm, and the surface (Fig. 5b–e) of the SCA displayed porous structures. Fig. 5f–j show SEM images of the cross-sectional structures of the SCA. As we expected, the densely packed fibrous network architecture extended inside the material, which proved that self-assembly of polymer chains is achieved in the slow-diffusion system through entanglement and physical crosslinking.[31]

Fig. 6 shows X-ray diffractograms (Fig. 6a) and DSC (Fig. 6b) of the chitosan powder (S0) and SCA (S1) samples. In the XRD patterns, three crystalline diffraction peaks were observed in S0, indexed as (020), (110), and (130) lattice diffraction of chitosan. However, (130) reflection peaks were not observed in S1, demonstrating that the molecular chain was reassembled during the reorganization process. As defined, the crystallinity index (CrI) is the degree of crystallinity of crystalline polymers, which describes the aggregation of molecular chains, and the distribution of crystal regions can affect toughness and mechanical strength.[19,28] In this work, the CrI obtained by software data fitting could reach more than 40%, surpassing the CrI of the powder, which was less than 10%; therefore, the SCA could be considered a highly crystalline polymer. The higher CrI also convincingly demonstrated that polymer chains were arranged in a more regular way. In the DSC tests, after the first heating to eliminate the heat history, the curves obtained from the second heating displayed that S0 undergoes glass transition at 93.82 °C. Glass transition is the process by which a substance changes from a glass state to a highly elastic state after the polymer absorbs energy;[22] the glass transition temperature of the chitosan powder indicates that the powder is amorphous or has low crystallinity. The S1 sample does not undergo glass transition even upon heating to the decomposition temperature. Combined with the XRD patterns and based on the conclusion described earlier, we can conclude that the synthesized sphere is a highly ordered and crystalline material.

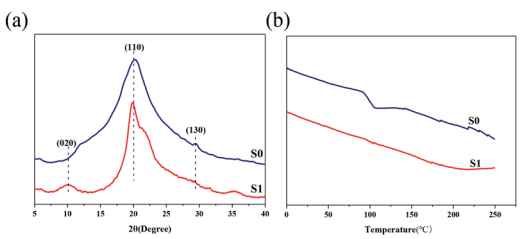

Fig. 6 X-ray diffraction patterns (a) and DSC curves (b) of chitosan powder and the SCA.

Mechanical properties

In our work, we used only mechanical characterization analysis of the adsorption resin to demonstrate the tolerance of the SCA for several reasons. Current studies on the preparation of chitosan spherical polymers by physical cross-linking are roughly classified into two categories: traditional acid dissolution methods and hydrogel cross-linking. The former only has the strength of the outer shell and is unable to withstand any pressure tests. The mechanical properties of the latter are determined by their compressive fracture stress and strain because of the need for strong mechanical properties and excellent flexibility during application in the field. However, the mechanical performance that these tests can reflect is far from sufficient compared with the actual applied strength of the adsorption resin. In our experiment, we assessed the mechanical properties of the SCA by calculating sphericity after attrition according to the Chinese national recommended standard. 50 mL of the SCA with sphere sizes ranging from 20–60 mesh were milled for 30 minutes. After drying and separation, the weight of the rounded and broken spheres was 9.9612 g and 1.1537 g respectively. The test result was calculated by formula (1), and the A of the SCA was 89.62%, indicating that the SCA has good mechanical properties even when swelled in aqueous solution.

After physical attrition and vibration in the machine, no changes in appearance, color or bead size were observed (Fig. 7b), indicating that the SCA is hard and tough. Only a small part was crushed and misshapen, demonstrating the impact toughness of the SCA (Fig. 7c). Based on the above results, we can conclude that the mechanical strength of the SCA reaches the standard for the practical application of commercial ion exchange resins.

Available functional groups and adsorption onto the SCA

To provide evidence that the available functional groups are obtained even on the formation of highly crystalline SCA materials, the content of amino groups was determined by titration. The ion exchange capacity Q of the dry resin ball was calculated by formula (2) and was in the range of 5.2–6.2 mmol g^{-1}. This result was in line with the total maximum amino capacity, which varied from 5.9 to 6.2 mmol g^{-1}, illustrating the availability of

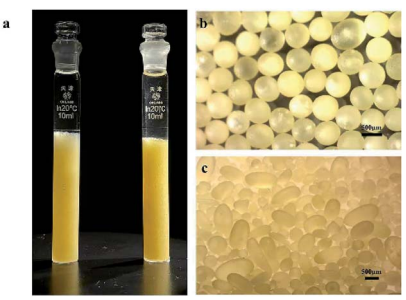

Fig. 7 The images of CSA that swelling in water before and after attrition (a), CSA samples tested after attrition (b) and magnified OM photomicrographs(c).

Table 1 Adsorption capacities of copper on various adsorbents

Adsorbent	Adsorption capacity	Adsorption time	pH	Temperature	Reference
SCA	200 mg g^{-1}	24 h	5.2	25 °C	—
Chitosan beads	33.44 mg g^{-1}	50 min	6	25 °C	Ngah, Kamari and Koay (2004)
Chitosan powder (75/110 μm)	45 mg g^{-1}	24 h	5	25 °C	Huang *et al.* (1995)
Chitosan powder (420/590 μm)	176 mg g^{-1}	5 days	5	25 °C	Juang *et al.* (1999)

functional groups and access to practical applications in various fields.

Research on the adsorption behaviours of the SCA involves evaluating the ability of highly crystalline SCA materials to adsorb metals from aqueous solution. In many studies, copper was selected as a coordination centre to combine with amino and hydroxyl groups. Thus, we compared the copper adsorption performance of the SCA with those reported for chitosan powder and physical cross-linked materials of different shapes. The adsorption conditions of the SCA were designed to be basically consistent with the control samples to ensure the credibility of the compared results.[32]

Table 1 shows the experimental conditions and the capacities of the SCA and the other chitosan samples in adsorbing Cu(II) ions. Obviously, the adsorption capacity of the SCA was significantly higher than the maximum content of the traditionally prepared chitosan particles and powders at equilibrium. In our preliminary experiment, the adsorption of the SCA with mesh sizes ranging from 20 to 60 was 81.8 mg g^{-1} for 8 h and then increased to 200 mg g^{-1} after 24 h, which was higher than the reported adsorption. As we mentioned earlier, the chitosan beads made by traditional physical methods were microparticles and had a high degree of surface cross-linking,[33] contributing to insufficient loading and a low possibility of diffusion and coordination. Chitosan power is at a distinct disadvantage in the mass transfer process to a certain degree.[34] When the particle size was increased and the concentration of acid was adjusted to make chitosan insoluble, the equilibrium amount reached 176 mg g^{-1}. However, this experimental process took 4–5 days, and there was a high cost of separation and regeneration.[35] It has been reported that the interaction speed of Cu(II) ions with coordination atoms is much faster than that of other metal ions.[36] As a result, a copper complex matrix tended to form quickly around the resin particles, hindering the diffusion of metal ions into the resin particles. Significantly, the SCA experienced a continuous increase in the amount of copper adsorbed within 24 hours, which finally reached a high level, confirming that the crystal region provided positive effects on the supports for its structure and the coordination and diffusion of the adsorption process. Therefore, this SCA is a biocompatible and biodegradable polymer material with high adsorption capacity and great future application potential in the field of adsorbent materials.

Conclusions

A new suspension dispersion-controllable polymerization system was developed to realize the orderly stacking and rearrangement of polymer chains, and an ultrahigh-strength spherical chitosan polymer adsorbent was successfully prepared through a green pathway. Based on the characteristic reorganization by alkalization of chitosan suspended in a solvent after acid dissolution, the molecular polymer chain reorganized regularly in the presence of the barrier and self-assembled to form a three-dimensional aggregated network structure by decreasing the polymerization rate. The excellent mechanical properties that were much higher than those of all reported non-composite chitosan polymers were certified by determining the sphericity after attrition, which indicated that the ultrahigh crystallinity of the SCA underpinned the entire spherical framework. In addition, the SCA exhibits excellent adsorption performance, including the availability of functional groups, mass transference and coordination ability, which were superior to those of other adsorption materials. Moreover, the SCA was purely physically cross-linked without any involvement of toxic reagents, ensuring the biocompatibility and biodegradation ability of the material. Therefore, this work is of great research significance for the biocompatibility and sustainable development of green chitosan resin construction for the field of adsorption materials.

Author contributions

Caihong Liu is role for conceptualization, data curation, formal analysis, writing – original draft. Chunhong Wang is role for resources, supervision, writing – review & editing. Haitao Jiang is role for investigation, methodology.

Conflicts of interest

The authors declare no competing financial interests.

Notes and references

1 P. Barbaro and F. Liguori, *Chem. Rev.*, 2009, **109**, 515–529.
2 D. Reichenberg, *J. Am. Chem. Soc.*, 2002, **75**, 589–597.
3 D. S. Cousins, B. Tan, J. Howell, Y. Suzuki, J. R. Samaniuk, D. M. Knauss and J. R. Dorgan, *ACS Sustainable Chem. Eng.*, 2019, **7**, 6512–6521.
4 J. Araki, Y. Yamanaka and K. Ohkawa, *Polymer*, 2012, **44**, 713–717.
5 W. Jiang, W. Wang, B. Pan, Q. Zhang, W. Zhang and L. Lv, *ACS Appl. Mater. Interfaces*, 2014, **6**, 3421–3426.
6 C. Kim, W. Choi and M. Choi, *ACS Appl. Mater. Interfaces*, 2019, **11**, 16586–16593.

7 K. Kurita, H. Ikeda, M. Shimojoh and J. Yang, *Polymer*, 2007, **39**, 945–952.
8 W. S. W. Ngah, L. C. Teong and M. A. K. M. Hanafiah, *Carbohydr. Polym.*, 2011, **83**, 1446–1456.
9 I. O. Saheed, W. D. Oh and F. B. M. Suah, *J. Hazard. Mater.*, 2021, **408**, 124889.
10 N. S. Surgutskaia, A. Di Martino, J. Zednik, K. Ozaltin, L. Lovecka, E. D. Bergerova, D. Kimmer, J. Svoboda and V. Sedlarik, *Sep. Purif. Technol.*, 2020, **247**, 116914.
11 X. Wang, L. Yang, J. Zhang, C. Wang and Q. Li, *Chem. Eng. J.*, 2014, **251**, 404–412.
12 H. Mittal, S. S. Ray, B. S. Kaith, J. K. Bhatia, Sukriti, J. Sharma and S. M. Alhassan, *Eur. Polym. J.*, 2018, **109**, 402–434.
13 N. Boucard, C. Viton and A. Domard, *Biomacromolecules*, 2005, **6**, 3227–3237.
14 B. Ding, H. Gao, J. Song, Y. Li, L. Zhang, X. Cao, M. Xu and J. Cai, *ACS Appl. Mater. Interfaces*, 2016, **8**, 19739–19746.
15 A. Montembault, C. Viton and A. Domard, *Biomacromolecules*, 2005, **6**, 653–662.
16 M. L. Pita-Lopez, G. Fletes-Vargas, H. Espinosa-Andrews and R. Rodriguez-Rodriguez, *Eur. Polym. J.*, 2021, **145**, 15–23.
17 J. Nie, W. Lu, J. Ma, L. Yang, Z. Wang, A. Qin and Q. Hu, *Sci. Rep.*, 2015, **5**, 7635.
18 Y. Xiong, K. Yan, W. E. Bentley, H. Deng, Y. Du, G. F. Payne and X. W. Shi, *ACS Appl. Mater. Interfaces*, 2014, **6**, 2948–2957.
19 J. J. Duan, X. C. Liang, Y. Cao, S. Wang and L. N. Zhang, *Macromolecules*, 2015, **48**, 2706–2714.
20 S. Ladet, L. David and A. Domard, *Nature*, 2008, **452**, 76–79.
21 M. F. Radwan, H. M. Dardeer, E. E. Elboray and M. F. Aly, *J. Mol. Struct.*, 2021, **1241**, 130625.
22 X. Shi, G. Zhang, T. V. Phuong and A. Lazzeri, *Molecules*, 2015, **20**, 1579–1593.
23 J. Wang, X. T. Hao, H. C. Yan, Q. Jiang, H. Y. Peng, B. J. Xiong, Y. G. Liao and X. L. Xie, *Polymer*, 2020, **188**, 122148.
24 A. C. Chao, S. H. Yu and G. S. Chuang, *J. Membr. Sci.*, 2006, **280**, 163–174.
25 K. Ravishankar and R. Dhamodharan, *React. Funct. Polym.*, 2020, **149**, 104517.
26 N. S. Surgutskaia, A. D. Martino, J. Zednik, K. Ozaltin, L. Lovecká, E. D. Bergerová, D. Kimmer, J. Svoboda and V. Sedlarik, *Sep. Purif. Technol.*, 2020, **247**, 116914.
27 J. Nie, Z. Wang and Q. Hu, *Sci. Rep.*, 2016, **6**, 36053.
28 X. Q. Wei, J. J. Duan, X. J. Xu and L. N. Zhang, *ACS Sustainable Chem. Eng.*, 2017, **5**, 3195–3203.
29 L. Xu, S. Gao, Q. Guo, C. Wang, Y. Qiao and D. Qiu, *Adv. Mater.*, 2020, **32**, e2004579.
30 Y. Zhang, C. Xue, Y. Xue, R. Gao and X. Zhang, *Carbohydr. Res.*, 2005, **340**, 1914–1917.
31 K. Yan, F. Ding, W. E. Bentley, H. Deng, Y. Du, G. F. Payne and X. W. Shi, *Soft Matter*, 2014, **10**, 465–469.
32 M. He, X. Wang, Z. Wang, L. Chen, Y. Lu, X. Zhang, M. Li, Z. Liu, Y. Zhang, H. Xia and L. Zhang, *ACS Sustainable Chem. Eng.*, 2017, **5**, 9126–9135.
33 W. S. Wan Ngah, A. Kamari and Y. J. Koay, *Int. J. Biol. Macromol.*, 2004, **34**, 155–161.
34 C. Huang, Y. Chung and M. Liou, *J. Hazard. Mater.*, 1996, **45**, 265–277.
35 R. S. Juang, F. C. Wu and R. L. Tseng, *Water Res.*, 1999, **33**, 2403–2409.
36 S. Kalyani, J. A. Priya, P. S. Rao and A. Krishnaiah, *Sep. Sci. Technol.*, 2005, **40**, 1483–1495.